
CONCURRENCE: A DEPENDENCE CRITERION FOR TIME SERIES, APPLIED TO BIOLOGICAL DATA

Evangelos Sariyanidi^{1*}, John D. Herrington^{1,2}, Lisa Yankowitz¹, Pratik Chaudhari²,
Theodore D. Satterthwaite², Casey J. Zampella¹, Jeffrey S. Morris²,
Edward Gunning², Robert T. Schultz^{1,2}, Russell T. Shinohara², Birkan Tunc^{1,2}

¹The Children’s Hospital of Philadelphia ²University of Pennsylvania

ABSTRACT

Measuring the statistical dependence between observed signals is a primary tool for scientific discovery. However, biological systems often exhibit complex non-linear interactions that currently cannot be captured without a priori knowledge or large datasets. We introduce a criterion for dependence, whereby two time series are deemed dependent if one can construct a classifier that distinguishes between temporally aligned vs. misaligned segments extracted from them. We show that this criterion, concurrence, is theoretically linked with dependence, and can become a standard approach for scientific analyses across disciplines, as it can expose relationships across a wide spectrum of signals (fMRI, physiological and behavioral data) without ad-hoc parameter tuning or large amounts of data.

1 INTRODUCTION

Measuring the statistical dependencies between biological signals is fundamental for understanding the complex interplay within and between molecular, neurobiological, and behavioral processes. The most common approach to quantifying dependence is using linear model-based statistics, with the Pearson correlation coefficient being the dominant metric (Tjøstheim et al., 2022). However, biological systems often exhibit interactions (Janson, 2012) that cannot be captured by linear models (He & Yang, 2021), such as cross-frequency coupling (Schmidt & O’Brien, 1997), threshold effects (Beltrami & Jesty, 1995), phase shifts (Tiesinga & Sejnowski, 2010), feedback systems (Beltrami & Jesty, 1995), or multi-scale interactions (Qu et al., 2011).

While linear models cannot comprehensively capture statistical dependence, linear and non-linear models together can. That is, if two time series x and y are dependent but uncorrelated, then there must be (non-linear) mathematical transformations f and g such that the transformed signals $f(x)$ and $g(y)$ are correlated (Rényi, 1959). However, the transformations that expose the dependence can be particular to each problem and difficult to identify when the compared signals are generated by complex or unknown mechanisms. The Hilbert-Schmidt Independence Criterion (Gretton et al., 2007) –which can be considered as a generalization of distance correlation (Székely et al., 2007; Sejdinovic et al., 2013)– or variants of canonical correlation analysis (Verbeek et al., 2003; Andrew et al., 2013) can, in principle, determine linear and non-linear dependence. However, these approaches are successful only if one can identify model parameters or kernels that expose the dependence (Hua & Ghosh, 2015; Gretton et al., 2012), which may not be possible or may require large samples (Zhuang et al., 2020; Marek et al., 2022). Alternatively, one may use analytical transformations such as Fourier or wavelet decomposition (Greenblatt et al., 2012; Fujiwara & Daibo, 2016; Schmidt et al., 2012), but the generalizability of this approach is limited, as there is no single transformation that works for all signals (Mallat, 2009; Vetterli et al., 2014). Moreover, analytical transformations pose family-wise error problems (Maraun & Kurths, 2004; Kramer et al., 2008) because they typically decompose each signal into multiple signals (e.g., frequency bands), and dependence can occur between any pair of decomposed signals (e.g., cross-frequency dependence). These issues are exacerbated when the compared signals are multi-dimensional and only a subset in one set of signals depends on an

*sariyanide@chop.edu

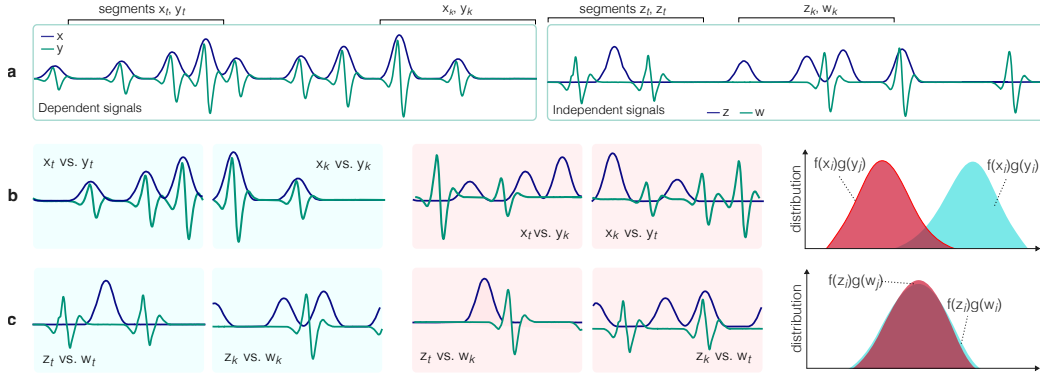


Figure 1: (a) Dependent signals x and y , and independent signals w and z . (b) Concurrent segments from x and y have different characteristics from non-concurrent segments, thus one can find functions f and g such that $f(x_i)g(y_j)$ is, on average, larger for concurrent segments (i.e., $i = j$) compared to non-concurrent segments (e.g., f as the identity operator and g the integral operator). (c) Concurrent and non-concurrent segments extracted from independent signals are not statistically distinguishable.

unknown subset in the other. In sum, currently there is no tractable method that can detect or quantify the dependence between a broad variety of biological signals when the dependence structure is not known a priori—presenting a major obstacle to scientific discovery.

We introduce a new approach, called *concurrency*, to quantify the statistical dependence between pairs of signals. The proposed approach is based on a simple idea: if two signals are statistically dependent, then temporally aligned (i.e., concurrent) segments of the compared signals are expected to be separable from segments that are temporally misaligned (i.e., not concurrent), as illustrated in Fig. 1. We show that this idea is not only intuitive, but also theoretically plausible, and it provides a straightforward and powerful recipe for automatically finding linear or non-linear transformations that expose dependence—namely, training a machine learning model that classifies between concurrent vs. non-concurrent segments from signals. Concurrency is essentially a contrastive learning (CL) approach that is not only used for representation learning, but also defines a bounded coefficient for statistical dependence (Section 2.3). That is, the proposed approach yields a score coined the concurrency coefficient, which is scaled between 0 and 1. Theoretical and experimental results indicate that this coefficient is proportional to the degree of dependence between the compared signals.

We apply concurrency to three distinct types of biological signals (i.e., fMRI, physiological, and behavioral data). Results suggest that concurrency can become a standard tool for scientific analyses, as it satisfies two critical priorities. First, the dependence in all compared biological signals as well as a large number of challenging synthetic datasets is detected without *any* ad-hoc hyperparameter modification, thus analyses can be conducted without the loss of power that would be caused by correcting for each tested parameter. Second, dependence can be detected even from modestly sized datasets without any pre-training, suggesting that concurrency can be applied in scientific domains where data is scarce or hard to obtain, or involve arbitrary types of sensors. We created an easy-to-use open-source software that implements concurrency, and runs efficiently on a single GPU. We will make this implementation publicly available should this paper be accepted for publication.

2 CONCURRENCE

Suppose that $x_{t,w}$ and $y_{t,w}$ are segments of signals x and y , observed between the time points t and $t + w$. If both $x_{t,w}$ and $y_{t,w}$ contain responses to a common event, then they must be statistically dependent. Thus, there must exist transformations f and g such that transformed representations of the segments, $f(x_{t,w})$ and $g(y_{t,w})$, are correlated (Rényi, 1959). The crux of our approach is that, while $f(x_{t,w})$ and $g(y_{t,w})$ are expected to be correlated, $f(x_{t,w})$ and $g(y_{t',w})$ are, on average, uncorrelated if t' is a random time point, different from t (Fig. 1b).

This idea is not only intuitive, but also theoretically plausible (Section 2.2), and provides a straightforward manner of detecting dependence automatically via self-supervision. Specifically, we quantify dependence via the *concurrency coefficient*, which is obtained by training a classifier (Section 2.1) to distinguish between concurrent vs. non-concurrent segments cropped randomly from a dataset of signal pairs, and calculating the normalized classification accuracy on another dataset $\mathcal{D} = \{(x^i, y^i)\}_i$:

$$\text{concurrency coefficient} = 2 \times \max(\text{accuracy}, 0.5) - 1. \quad (1)$$

The concurrency coefficient is bounded between 0 and 1, and its magnitude is proportional to the degree of dependence between the compared signal pairs (Section 2.2 and Fig. 2). The dataset \mathcal{D} must not overlap with the dataset used during training, lest the classifier may overfit and overestimate the dependence. Thus, one may use cross-validation (CV) and compute the average concurrency coefficient over the test sets of CV folds, or compute the concurrency coefficient on independent data.

2.1 THE LOSS FUNCTION AND THE PER-SEGMENT CONCURRENCE SCORE

The classifier that we use to compute the concurrency coefficient is a neural network that produces a *per-segment concurrence score* (PSCS) from segments $x_{t,w} \in \mathbb{R}^{K_x \times w}$ and $y_{t',w} \in \mathbb{R}^{K_y \times w}$, where K_x and K_y are the dimensions of x and y . The two segments are deemed concurrent if the PSCS is positive, and not concurrent if it is nonpositive. The PSCS is computed by first transforming the input segments via separate learned functions f and g into segments of dimensions K_f and K_g ,

$$f : \mathbb{R}^{K_x \times w} \rightarrow \mathbb{R}^{K_f \times w'}, \quad g : \mathbb{R}^{K_y \times w} \rightarrow \mathbb{R}^{K_g \times w'} \quad (2)$$

where w' is the temporal length of the transformed segments; then computing the covariance of the transformed segments, $C = \text{Cov}(f(x_{t,w}), g(y_{t',w}))$; and finally calculating the weighted average of the entries of the covariance matrix

$$s = \sum_i \sum_j \alpha_{ij} C_{ij}, \quad (3)$$

where C_{ij} is the ij th entry of C . The weights α_{ij} , as well as the transformations f and g , are learned from scratch while training the network. The loss function is simply the binary cross entropy (with logits), which is used to classify between PSCS values computed from randomly extracted concurrent segments ($t = t'$) versus non-concurrent segments ($t \neq t'$).

In addition to computing the concurrency coefficient, the PSCS can also be used one to quantify the dependence between a specific pair of segments. As such, the concurrency coefficient and the PSCS have two distinct uses for scientific analyses. While the concurrency coefficient can uncover whether and to what extent two processes (e.g., breathing rate and cardiac activity) are related in general (i.e., at the sample level), the PSCS between specific pairs of concurrent segments (i.e., $t = t'$) can uncover whether this relationship is stronger for a specific individual, for individuals with a certain condition (e.g., anxiety), or for certain moments within the compared signals. Our experiments on real data include use cases for both the concurrency coefficient and the PSCS.

2.2 THEORETICAL RELATION BETWEEN DEPENDENCE AND CONCURRENCE

We theoretically show that if the pairs of signals in \mathcal{D} are statistically dependent, then concurrent segments extracted from them are expected to be separable from non-concurrent segments. Moreover, the degree of separability increases with the degree of dependence between the signals, and with the segment size w . For tractability, our theoretical analysis relies on some simplifying assumptions—that the signals rely on stationary (Bernoulli) processes, and that there is no time lag between the dependent signals. Nevertheless, even these assumptions lead to challenging cases of non-linear dependence (Appendix E), and numerical simulations (Appendix C) and experiments with synthetic data show that the results of the theoretical analysis hold even when these assumptions are violated.

Suppose that the signals x^i and y^i in \mathcal{D} are realizations of respective discrete-time random sequences (RSs) $\mathbf{x}[t]$ and $\mathbf{y}[t]$ that are generated by convolving two binary RSs $\mathbf{h}_x[t]$ and $\mathbf{h}_y[t]$ with kernels $k_1[t]$ and $k_2[t]$, and adding noise processes $\mathbf{n}_x[t]$ and $\mathbf{n}_y[t]$ (Supp. Fig. E.1):

$$\mathbf{x}[t] = (\mathbf{h}_x \star k_1)[t] + \mathbf{n}_x[t] \quad (4)$$

$$\mathbf{y}[t] = (\mathbf{h}_y \star k_2)[t] + \mathbf{n}_y[t]. \quad (5)$$

The noise processes $\mathbf{n}_x[t]$ and $\mathbf{n}_y[t]$ are assumed to be independent from each other and from $\mathbf{h}_x[t]$ or $\mathbf{h}_y[t]$. The processes $\mathbf{h}_x[t]$ and $\mathbf{h}_y[t]$ are modeled as the product of a common process $\mathbf{h}[t]$ with two separate and independent processes $\alpha[t]$ and $\beta[t]$ that take binary values (0 or 1):

$$\mathbf{h}_x[t] = \alpha[t]\mathbf{h}[t] \quad (6)$$

$$\mathbf{h}_y[t] = \beta[t]\mathbf{h}[t], \quad (7)$$

where $\mathbf{h}[t]$, $\alpha[t]$ and $\beta[t]$ are Bernoulli processes with respective parameters p , p_α , p_β . The common process $\mathbf{h}[t]$ ensures that $\mathbf{x}[t]$ and $\mathbf{y}[t]$ are dependent, provided that $p \neq 0$, $p_\alpha \neq 0$ and $p_\beta \neq 0$. The processes $\alpha[t]$ and $\beta[t]$ make the dependence stochastic when $p_\alpha, p_\beta \in (0, 1)$, as the latter implies that only an a priori unknown set of events (i.e., $\mathbf{h}[t] = 1$) will be observed both in $\mathbf{x}[t]$ and in $\mathbf{y}[t]$.

Simple metrics such as correlation may be unable to expose even a deterministic dependence between \mathbf{x} and \mathbf{y} , as the kernels k_1 and k_2 can make the dependence non-linear. If one could recover the underlying binary processes \mathbf{h}_x and \mathbf{h}_y , one could simply compute the inner product of these two processes to expose dependence. While perfect recovery may not be realistic (e.g., due to noise \mathbf{n}_x and \mathbf{n}_y), one can assume that there exist estimators $\tilde{\mathbf{h}}_x$ and $\tilde{\mathbf{h}}_y$ that estimate these binary events (e.g., through deconvolution) up to additive error terms $\epsilon_x[t]$ and $\epsilon_y[t]$ as

$$\tilde{\mathbf{h}}_x[t] = \min\{\alpha[t]\mathbf{h}[t] + \epsilon_x[t], 1\} \quad (8)$$

$$\tilde{\mathbf{h}}_y[t] = \min\{\beta[t]\mathbf{h}[t] + \epsilon_y[t], 1\}, \quad (9)$$

where $\epsilon_x[t]$ and $\epsilon_y[t]$ are Bernoulli processes with respective parameters p_x^ϵ and p_y^ϵ , and the $\min\{\cdot\}$ operator ensures that $\tilde{\mathbf{h}}_x[t]$ and $\tilde{\mathbf{h}}_y[t]$ is a binary RS. The theorem below expresses that if \mathbf{x} and \mathbf{y} are dependent, then the inner product between $\tilde{\mathbf{h}}_x$ and $\tilde{\mathbf{h}}_y$ is larger when computed when these processes are temporally aligned compared to when they are misaligned.

Theorem 1. *Suppose that $\mathbf{z}(\tau)$ is an RV defined as a function of a temporal lag parameter τ as*

$$\mathbf{z}(\tau) = \frac{1}{w} \sum_{t=1}^w \min\{\alpha[t]\mathbf{h}[t] + \epsilon_x[t], 1\} \min\{\beta[t+\tau]\mathbf{h}[t+\tau] + \epsilon_y[t+\tau], 1\}, \quad (10)$$

where \mathbf{h} , α , β , ϵ_x and ϵ_y are Bernoulli processes with respective parameters p , p_α , p_β , p_x^ϵ and p_y^ϵ such that

$$p \in (0, 1), \quad p_\alpha, p_\beta \in (0, 1], \quad \text{and} \quad p_x^\epsilon, p_y^\epsilon \in [0, 1). \quad (11)$$

Further, suppose that \mathbf{z}^+ and \mathbf{z}^- are RVs derived from $\mathbf{z}(\tau)$ by respectively setting τ to zero and to a fixed and nonzero value $\tau' \neq 0$:

$$\mathbf{z}^- = \mathbf{z}(\tau'), \quad \mathbf{z}^+ = \mathbf{z}(0). \quad (12)$$

Then, $\mathbb{E}\{\mathbf{z}^+\} > \mathbb{E}\{\mathbf{z}^-\}$ for any time window $w \in \mathbb{Z}^+$, and the difference between the two means is

$$\mathbb{E}\{\mathbf{z}^+\} - \mathbb{E}\{\mathbf{z}^-\} = p(1-p)p_\alpha p_\beta (1-p_x^\epsilon)(1-p_y^\epsilon). \quad (13)$$

Moreover, there exists a threshold θ such that $P\{\mathbf{z}^+ < \theta\} \rightarrow 0$ and $P\{\mathbf{z}^- > \theta\} \rightarrow 0$ as $w \rightarrow \infty$.

The proof is provided in Appendix B. Theorem 1 implies that one can predict beyond chance level if segments extracted from the signal pairs in \mathcal{D} are concurrent or not, as the distribution of the \mathbf{z}^+ is not fully overlapping with that of \mathbf{z}^- (Supp. Fig. C.2). Also, the concurrence coefficient is expected to be proportional to the degree of dependence between the compared segments, as the difference in equation 13 increases with p_α and p_β . The latter difference decreases as p_x^ϵ and p_y^ϵ increases, thus the concurrence coefficient is expected to be inversely related to the amount of noise. Finally, the concurrence coefficient is expected to also increase with the segment size, as the overlap between the distributions of \mathbf{z}^+ and \mathbf{z}^- decreases with increasing w . The exact w value is expected to have little significance for exposing dependence, as the distributions of \mathbf{z}^+ and \mathbf{z}^- are theoretically separable for any positive w . Experiments on synthetic data corroborate this theoretical analysis (Fig. 2).

2.3 COMPARISON WITH OTHER CONTRASTIVE LEARNING APPROACHES

Concurrence relies on CL, and it is by no means the first CL approach on time series (Zhang et al., 2024). However, its goal and operation are fundamentally different from existing approaches, which

typically use CL for learning a representation that can be used for system identification (Hyvarinen & Morioka, 2016); or for downstream tasks, such as classification, forecasting, clustering or anomaly detection (Woo et al., 2022; Zhang et al., 2022; Tonekaboni et al., 2021; Oord et al., 2018; Tian et al., 2020). In contrast, the primary contribution of our work is to show that our CL criterion (i.e., concurrence) provides a principled and naturally bounded metric of statistical dependence for time series—a metric that is suitable for scientific analyses, as it exposes a wide range of dependencies without requiring users with deep learning expertise, large amounts of data or ad-hoc parameter tuning.

3 IMPLEMENTATION

Network architecture. To make the concurrence approach useful for scientific purposes, the functions f and g should be flexible enough to expose arbitrary dependencies. Also, one needs a training procedure that requires no hyperparameter tuning and can work successfully even with modestly-sized datasets, since the samples used in scientific analyses often have only hundreds or even fewer samples. As such, we model the transformations f and g with Convolutional Neural Networks (CNNs), which are universal approximators (Zhou, 2020) and, thanks to advances in machine learning (Wang et al., 2016; Bai et al., 2018), have well-established recipes for training across a large variety of temporal analysis tasks without ad-hoc modifications (Wang et al., 2016), particularly when modeling short-term dependencies (Bai et al., 2018). Our experiments with real and synthetic data verify that CNNs with the *same parameters* (Appendix A) can detect a wide range of linear or non-linear dependence patterns between signals that have distinct frequency characteristics and are corrupted by large amounts of noise. Further, the training does not require an unrealistic sample size, as our experiments show that even fewer than 100 signal pairs can suffice.

Significance testing. We advise using significance tests to avoid false discoveries (i.e., Type I error), particularly when the concurrence coefficient is computed on small samples. Specifically, we recommend permutation tests (Nichols & Holmes, 2002) where the null distribution is constructed from concurrence coefficients computed after randomly re-assigning the labels of segments pairs (i.e., concurrent/non-concurrent). Our analyses (Appendix D) show that such tests can be conducted efficiently by using a relatively small number (e.g., 1000 or fewer) of permutations (Winkler et al., 2016) and leveraging a Pearson Type III approximation (Kazi-Aoual et al., 1995).

Computational complexity. The complexity of our implementation is $\mathcal{O}(Nw(K_x + K_y))$, where N is the number of signals used for training the classifier. As a reference, computing the concurrence coefficient for each of the synthesized datasets ($T = 1000$, $N = 400$, $w = 400$; see Section 4.2) takes approximately 40 seconds on a single NVIDIA RTX 3090 GPU.

4 EXPERIMENTAL VALIDATION

We first investigate whether the theoretically expected properties of concurrence hold in practice. Next, we compare concurrence with eight alternative methods on a large number of synthesized datasets. Finally, we apply concurrence on three types of real data with single- and multi-dimensional signals that are dependent linearly or non-linearly, namely brain imaging (fMRI), physiological (breathing and heart rate), and behavioral (facial expressions and head movements) signals.

4.1 MEASURING STOCHASTIC DEPENDENCE, AND THE EFFECT OF SEGMENT SIZE

Biological signals may depend on each other stochastically rather than deterministically, as they typically reflect an admixture of multiple processes, and only a subset of these processes may be dependent between compared signals. Another cause of non-deterministic dependence is measurement noise, which can overpower the compared signals (Welvaert & Rosseel, 2013).

Fig. 2a simulates scenarios where the degree of dependence is controlled with a parameter ξ , which varies between 0 (independent signal pairs) and 1 (completely dependent signal pairs). Fig. 2c shows the concurrence coefficients obtained from pairs of signals with varying degrees of dependence (i.e., ξ). Results show that the concurrence coefficient successfully detects dependencies ($\xi > 0$) and lack thereof ($\xi = 0$). Of note, the concurrence coefficient is approximately linearly proportional to ξ when w is large enough to contain the entire dependence event (e.g., $w = 100$ for signals in

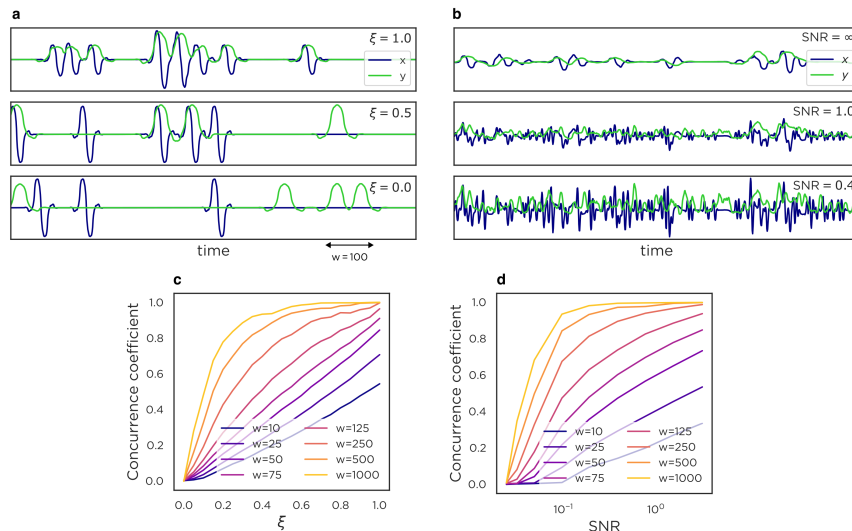


Figure 2: (a) Synthesized signals with deterministic dependence ($\xi = 1.0$), stochastic dependence ($\xi = 0.5$) and no dependence ($\xi = 0.0$). (b) Dependent pairs of signals with varying degrees of noise. (c) Concurrence coefficient vs. ξ (d) Concurrence coefficient vs. signal-to-noise ratio (SNR).

Fig. 2a) but not much larger. While the degree of dependence ξ is overestimated with larger segments, there is no risk of detecting spurious relationships (false positives), as the concurrence coefficient remains approximately zero when $\xi = 0$, regardless of w . Fig. 2d shows that concurrence can also handle noise. The concurrence coefficient usually decreases with the signal-to-noise (SNR), yet it can uncover dependence even when the SNR is 0.10, which is lower than a worst-case estimate of noise in fMRI data (SNR=0.35; see Welvaert & Rosseel (2013)).

4.2 COMPARISON WITH ALTERNATIVE METHODS

We generated 100 synthetic datasets, where each dataset contained pairs of statistically dependent signals. The goal was to determine the dependence in as many datasets as possible by using only the off-the-shelf implementation of our algorithm, without any ad-hoc parameter adjustment. The datasets were designed to be challenging, with dependencies difficult to visually ascertain (Fig. 3).

Datasets. Each of the 100 synthesized datasets is comprised of 500 pairs of signals (x, y) generated by convolving a randomly generated binary signal with a randomly determined kernel, akin to equations 4 and 5. Specifically, the kernels were randomly chosen wavelets (at random scales) from the `pywavelets` library, typically resulting in non-linear dependence. To test the algorithm in the presence of non-stationarity, the produced binary signals were made non-stationary, with the probability of observing an event increased or decreased linearly over time at a random rate. To simulate lagged dependence, one of the signals in each pair was also shifted (circularly) by a random lag between 0 and 50 time frames. We also added noise to each signal, by generating it in a similar way—namely, by convolving randomly selected kernels with separate and independent binary signals.

Compared methods. We compared concurrence with correlation (Pearson’s r), windowed cross-correlation (WCC) (Boker et al., 2002), distance correlation (DC) (Székely et al., 2007), Hilbert-Schmidt Independence Criterion (HSIC) (Gretton et al., 2007), Mutual Information (MI), Conditional MI (CMI), Multiscale Graph Correlation (MGC), Kernel Mean Embedding Random Forest (KMERF). HSIC, MGC and KMERF have been implemented via the `hyppo` software package; DC was implemented via `dcor` (Ramos-Carreño, 2022); and Pearson’s r was implemented through `scikit-learn`. We provided our own implementation for the remaining methods. The statistical significance for all methods have been computed via permutation tests. Concurrence coefficient was computed on 20% of each dataset, after using 80% of data for training.

Results. Table 1 shows the results of experiments on synthesized data. CMI is the best among methods alternative to concurrence, due possibly to its ability to model non-linear dependence and

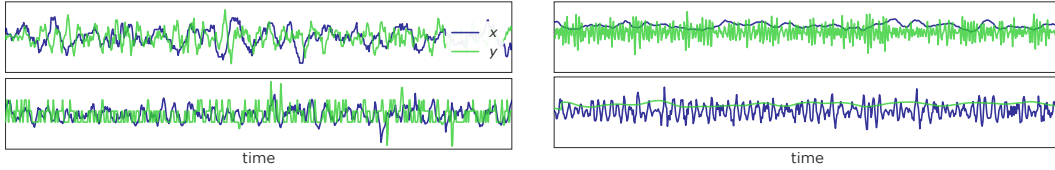


Figure 3: Pairs of (dependent) signals from six of the 100 synthesized datasets used in experiments. Dependence is typically not easy to visually ascertain.

Table 1: Results from the 100 synthetic datasets: The number of datasets that have been (correctly) identified as statistically dependent (at significance level 0.05) by each of the compared methods.

Pearson’s r	WCC	DC	HSIC	MI	CMI	MGC	KMERF	Concurrence
8	10	12	10	7	34	9	11	97

temporal dependence, yet can detect the dependence in only 34% of the datasets. All alternative methods can possibly detect the dependence in more datasets if their parameters are optimized for each dataset. However, this is often not feasible for scientific analyses with modestly sized datasets, as one should do multiple tests correction (Armstrong, 2014) for the tested parameter values, leading to significant decrease in statistical power. Concurrence detected the dependence in 97% of datasets, using identical hyperparameters (Appendix A) and segment size ($w = 400$).

4.3 APPLICATIONS TO REAL BIOLOGICAL SIGNALS

Brain Imaging Our experiments on fMRI signals aim to identify how strongly different brain regions are functionally connected. Pearson’s r is the single-most commonly used metric for this purpose (Liu et al., 2024). Fig. 4 compares the connectivity matrices obtained with Pearson’s r (i.e., correlation matrix) and the concurrence coefficient (i.e., concurrence matrix) on a version of the Philadelphia Neurodevelopmental Cohort dataset (Baum et al., 2020) that was pre-processed as in prior work (Satterthwaite et al., 2016). This dataset uses the parcellation scheme that divides each brain into 400 regions (Schaefer et al., 2018). The concurrence coefficient is computed on segments of size $w = 30$ time points, which corresponds to approximately 90 seconds, whereas the entire signals included 120 time points. Thirty percent of the dataset (426 participants) was used to train the neural networks needed for the concurrence coefficients, and the results in both connectivity matrices were computed from the remaining 70%. The overall similarity between the two connectivity matrices (Fig. 4c vs. Fig. 4d) is striking and suggests that the concurrence coefficient uncovers a dependence structure that has been validated in the field. Fig. 4g shows that there are no pairs of regions with a concurrence score less than 0.2, even though there are many pairs that are uncorrelated (i.e., Pearson $r \approx 0$), suggesting that concurrence captured statistical dependencies that cannot be captured with correlation (e.g., Fig. 4b) as well as those that can (e.g., Fig. 4a). The fact that the concurrence coefficient exposed a dependence between all $400 \times 199 = 79,600$ pairs of brain regions with 79,600 independently trained networks verifies that the training needed for concurrence can be done robustly. We ran a permutation test to identify if the method detects spurious dependence (Type I error) by computing concurrence between signals of mismatched participants. The concurrence coefficient was closely distributed around zero (Fig. 4h), indicating no spurious relationships. The differences between the concurrence coefficient and Pearson’s correlation exhibit a structured pattern across the seven brain networks (Fig. 4F), increasing progressively from lower-order affective (limbic), somatomotor and sensory (visual) networks to higher-order cognitive control (ventral attention, dorsal attention, default mode, frontoparietal) networks. This systematic increase suggests that linear correlation may not be capturing complex connectivity patterns that involve integrative processing or dynamic modulation.

Physiological data. We next investigate dependencies in a dataset of breathing and cardiac activity. While these two processes are known to be biologically linked (Adrian et al., 1932), the correlation between respiration rate and electrocardiogram (ECG) signals is approximately zero (Fig. 5a). We applied the proposed method to a dataset of 60 pairs of temporally synchronized ECG and respiration rate signals, collected at the Children’s Hospital of Philadelphia using Zephyr BioModule sensors. The duration of the tasks used for data collection ranged from 4 to 7 minutes. The data were split into

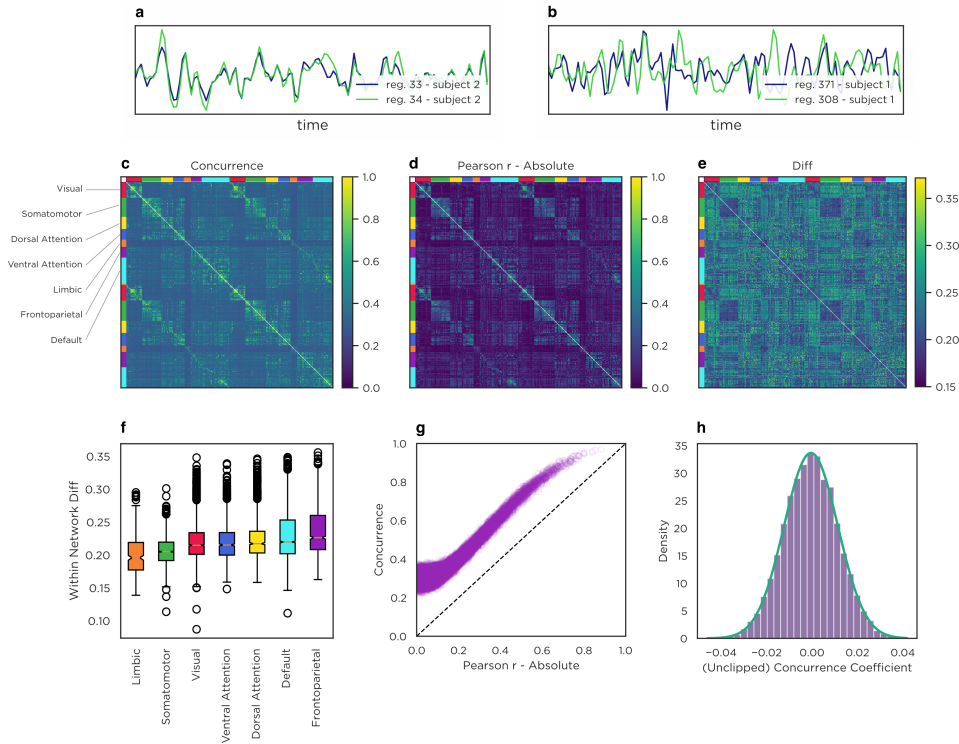


Figure 4: (a) Correlated fMRI signals from two brain regions. (b) Signals from regions that are dependent (concurrence coefficient: 0.25) but uncorrelated (Pearson’s r : 0.02). (c) Connectivity matrix computed with the concurrence coefficient. (d) Connectivity matrix computed with (absolute) Pearson’s r values. (e) The difference between the concurrence- and correlation-based connectivity matrices. (f) The distributions of the difference between the concurrence- and correlation-based connectivity matrices, shown separately for the seven brain networks. (g) Comparison of the Pearson’s r vs. concurrence coefficients computed from all the brain region pairs. (h) The (unclipped) concurrence coefficient between 10,000 pairs of brain regions of mismatched participants.

four subject-independent cross-validation folds. The segment size w was equivalent to 5 seconds. The average concurrence coefficient on the test folds was 0.50 ($p < 0.001$), indicating that the concurrence approach successfully detects the relationship between respiration rate and ECG signals. The PSCS can generally distinguish between compared signals that are temporally aligned or not (Fig. 5b-d), validating that concurrence can identify relationships (or lack thereof) that are difficult to determine visually. Fig. 5e plots the PSCSs from temporally aligned segments vs. the root mean square of successive differences (RMSSD) derived from the ECG signal of each interaction. That the PSCS is generally larger when the RMSSD is low may suggest that the trained algorithm predicts a stronger relationship between ECG and respiration rate when the latter is increased.

Behavioral Data. Finally, we apply concurrence to the analysis of facial behavior in a dyadic conversation. The behaviors of two conversation partners are expected to be dependent, due to well-known phenomena like nonconscious mimicry (Lakin et al., 2003) or (nonverbal) backchanneling (Shelley & Gonzalez, 2013). However, quantifying such dependencies has proven challenging, as behavior is captured with multi-dimensional signals (Supp. Fig. F.1), and any subset of signals from one conversation partner may depend on the signals of the other partner through an unknown relationship. We conduct experiments on a dataset of 199 participants (aged 5 to 40 years) engaged in a 3-5-minute semi-structured face-to-face conversation (Sariyanidi et al., 2023). We quantify social behaviors (i.e., facial expressions and head movements) in each conversation partner with 82-dimensional signals (79 for facial expressions and 3 for head movements) (Sariyanidi et al., 2024). The concurrence coefficient for $w = 4$ seconds is 0.49 ($p < 0.001$), indicating that the behavior signals of the conversation partners are dependent. Moreover, the PSCS allows us to investigate differences within different subsamples. For example, PSCS increases with age (Spearman’s $r = 0.61$, $p < 0.001$; Supp. Fig. F.1c),

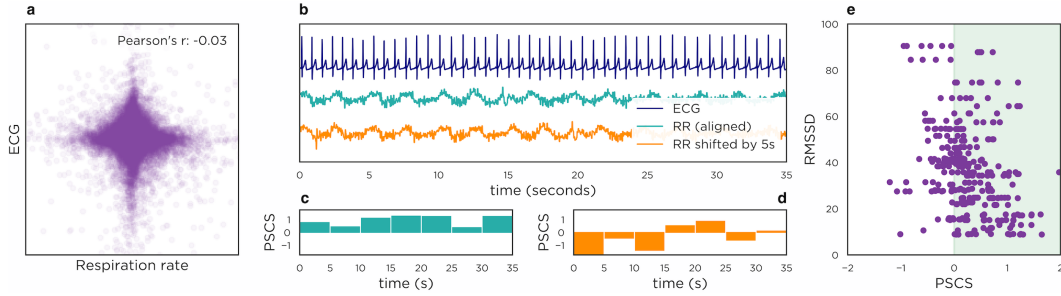


Figure 5: (a) Scatter plot and correlation between the respiration rate (RR) and ECG signal. (b) A sample ECG signal plotted against the synchronized (i.e., time-aligned) RR signal and the temporally misaligned RR. (c) The per-segment concurrence scores (PSCSs) between the temporally aligned ECG and RR are positive, which indicate that the PSCS correctly predicts that the segments are temporally aligned. (d) The PSCSs between the temporally misaligned ECG and RR are generally negative. (e) The PSCS for (temporally aligned) ECG and RR signals against the RMSSD, computed on a dataset of 30 participants for multiple segments per participant.

indicating that younger school-age children tend to have less behavioral coordination than older children. Additional analyses on a subsample of 12-18 year-olds ($N=42$) with and without an autism diagnosis (matched on age and sex) indicate that autistic adolescents have reduced coordination with conversation partners relative to neurotypical adolescents (Cohen's D : 0.8; $p=0.003$; Supp. Fig. F.1c). These results show that concurrence exposes clinically relevant differences in spontaneous behavioral coordination, without any a priori information about the structure of the coordination.

5 LIMITATIONS AND FUTURE WORK

We showed that the concurrence coefficient is proportional to the degree of dependence between the compared signals. However, one must exercise caution when making comparative judgments to ascertain whether a pair of processes are more strongly related than another pair, since the concurrence coefficient can be made larger by simply increasing the segment size w (Section 2.2; Fig. 2c,d). As such, w must be chosen in a way that the comparisons are commensurate. Nevertheless, the choice of w is of little concern if one aims to ascertain whether two processes are dependent or not.

Our theoretical analyses relied on simplifying assumptions for analytical tractability. However, the proposed framework can be used beyond these assumptions. For example, the physiological signals in our experiments are highly periodic, which violates the (Bernoulli) assumption that consecutive dependence events are independent of one another (Bertsekas & Tsitsiklis, 2008). A critical future direction is to precisely delineate the dependencies that can be exposed through concurrence by relaxing or eliminating these assumptions. Finally, we implemented concurrence via CNNs as they are easy to train. However, in the presence of long-range relationships, CNNs may require parameter modification (Appendix A) or fail, whereas architectures such as transformers are highly capable in this scenario. The research by the machine learning community can lead to streamlined and efficient training procedures for more modern architectures, enabling their usage with concurrence.

6 CONCLUSION

We introduced a new approach for measuring statistical dependence in time series, namely, concurrence. We showed that constructing a binary classifier that simply distinguishes between concurrent and non-concurrent segments of the compared time series leads to a theoretically supported and practically potent framework. Concurrence can become a standard way of quantifying statistical dependence between time series, as it readily detects a wide range of linear or non-linear dependencies with an off-the-shelf implementation, even from modestly sized samples and noisy data, without requiring empirical (hyper)parameter tuning; showed no propensity to false discoveries (Type I errors), and works with single- or multi-dimensional signals. Future research can further enhance this framework by theoretically establishing the most general conditions under which concurrence exposes

dependence, while integrating new architectures and well-established training recipes developed by the machine learning community can ensure that its theoretical potential can be fully actualized.

REFERENCES

- Edgar D. Adrian, Detlev W. Bronk, and G. Phillips. Discharges in mammalian sympathetic nerves. *The Journal of Physiology*, 74:115–133, 1932.
- Galen Andrew, Raman Arora, Jeff Bilmes, and Karen Livescu. Deep canonical correlation analysis. In *Proceedings of the 30th International Conference on Machine Learning (ICML)*, 2013.
- Richard A Armstrong. When to use the Bonferroni correction. *Ophthalmic and physiological optics*, 34(5):502–508, 2014.
- Shaojie Bai, J. Zico Kolter, and Vladlen Koltun. An empirical evaluation of generic convolutional and recurrent networks for sequence modeling. arXiv:1803.01271, 2018. URL <https://doi.org/10.48550/arXiv.1803.01271>.
- Graham L. Baum, Zhen Cui, David R. Roalf, Rastko Ciric, Richard F. Betzel, Barron Larsen, Matthew Cieslak, Philip A. Cook, Chun H. Xia, Tyler M. Moore, Kosha Ruparel, David J. Oathes, Aaron F. Alexander-Bloch, Russell T. Shinohara, Armin Raznahan, Raquel E. Gur, Ruben C. Gur, Danielle S. Bassett, and Theodore D. Satterthwaite. Development of structure–function coupling in human brain networks during youth. *Proceedings of the National Academy of Sciences*, 117:771–778, 2020.
- Edward Beltrami and John Jesty. Mathematical analysis of activation thresholds in enzyme-catalyzed positive feedbacks: application to the feedbacks of blood coagulation. *Proceedings of the National Academy of Sciences of the USA*, 92:8744–8748, 1995.
- Dimitri Bertsekas and John N. Tsitsiklis. *Introduction to Probability*. Athena Scientific, 2008.
- Steven M Boker, Jennifer L Rotondo, Minquan Xu, and Kadajah King. Windowed cross-correlation and peak picking for the analysis of variability in the association between behavioral time series. *Psychological methods*, 7(3):338, 2002.
- Katsunori Fujiwara and Ikuo Daibo. Evaluating interpersonal synchrony: Wavelet transform toward an unstructured conversation. *Frontiers in Psychology*, 7, 2016.
- Robert E. Greenblatt, Mary E. Pfeieger, and Alexei E. Ossadtchi. Connectivity measures applied to human brain electrophysiological data. *Journal of Neuroscience Methods*, 207:1–16, 2012.
- Arthur Gretton, Kenji Fukumizu, Choon H. Teo, Le Song, Bernhard Schölkopf, and Alexander J. Smola. A kernel statistical test of independence. In *Advances in Neural Information Processing Systems 20 (NIPS 2007)*, 2007.
- Arthur Gretton, Dino Sejdinovic, Heiko Strathmann, Sivaraman Balakrishnan, Massimiliano Pontil, Kenji Fukumizu, and Bharath K. Sriperumbudur. Optimal kernel choice for large-scale two-sample tests. In *Advances in Neural Information Processing Systems 25*. Curran Associates, Inc., 2012.
- Fei He and Yuguo Yang. Nonlinear system identification of neural systems from neurophysiological signals. *Neuroscience*, 458:213–228, 2021.
- Wei-Yi Hua and Debashis Ghosh. Equivalence of kernel machine regression and kernel distance covariance for multidimensional phenotype association studies. *Biometrics*, 71:812–820, 2015.
- Aapo Hyvarinen and Hiroshi Morioka. Unsupervised feature extraction by time-contrastive learning and nonlinear ica. *Advances in neural information processing systems*, 29, 2016.
- Natalia B. Janson. Non-linear dynamics of biological systems. *Contemporary Physics*, 53:137–168, 2012.
- F. Kazi-Aoual, S. Hitier, R. Sabatier, and J.-D. Lebreton. Refined approximations to permutation tests for multivariate inference. *Computational Statistics & Data Analysis*, 20:643–656, 1995.

-
- Mark A. Kramer, Adriano B. L. Tort, and Nancy J. Kopell. Sharp edge artifacts and spurious coupling in eeg frequency comodulation measures. *Journal of Neuroscience Methods*, 170:352–357, 2008.
- Jessica L. Lakin, Victoria E. Jefferis, C. M. Cheng, and Tanya L. Chartrand. The chameleon effect as social glue: Evidence for the evolutionary significance of nonconscious mimicry. *Journal of Nonverbal Behavior*, 27:145–162, 2003.
- Zheng-Quan Liu, Andrea I. Luppi, Jesper Y. Hansen, Yue E. Tian, Andrew Zalesky, B. T. Thomas Yeo, Ben D. Fulcher, and Bratislav Mišić. Benchmarking methods for mapping functional connectivity in the brain. bioRxiv 2024.05.07.593018, 2024. URL <https://doi.org/10.1101/2024.05.07.593018>.
- Stéphane Mallat. *A Wavelet Tour of Signal Processing: The Sparse Way*. Academic Press, 3 edition, 2009.
- David Maraun and Jürgen Kurths. Cross wavelet analysis: significance testing and pitfalls. *Nonlinear Processes in Geophysics*, 11:505–514, 2004.
- Scott Marek, Brenden Tervo-Clemmens, Finnegan J. Calabro, Daniel F. Montez, Benjamin P. Kay, Alexander S. Hatoum, Mary R. Donohue, William Foran, Ryan L. Miller, Timothy J. Hendrickson, Shane M. Malone, Suyash Kandala, Eric Feczko, Oscar Miranda-Dominguez, Amy M. Graham, Eric A. Earl, Alex J. Perrone, Miguel Cordova, Owen Doyle, Lily A. Moore, Grace M. Conan, Juan Uriarte, Kyle Snider, Benjamin J. Lynch, Jordan C. Wilgenbusch, Taylor Pengo, Angela Tam, Jiayu Chen, D. J. Newbold, Alexander Zheng, Nicholas A. Seider, Ahria N. Van, Asuka Metoki, R. J. Chauvin, Timothy O. Laumann, Deanna J. Greene, Steven E. Petersen, Hugh Garavan, Wesley K. Thompson, Thomas E. Nichols, B. T. T. Yeo, Deanna M. Barch, Beatriz Luna, Damien A. Fair, and N. U. F. Dosenbach. Reproducible brain-wide association studies require thousands of individuals. *Nature*, 603:654–660, 2022.
- Thomas E. Nichols and Andrew P. Holmes. Nonparametric permutation tests for functional neuroimaging: a primer with examples. *Human Brain Mapping*, 15:1–25, 2002.
- Aaron van den Oord, Yazhe Li, and Oriol Vinyals. Representation learning with contrastive predictive coding. *arXiv preprint arXiv:1807.03748*, 2018.
- Zhilin Qu, Alan Garfinkel, James N. Weiss, and Mikko Nivala. Multi-scale modeling in biology: How to bridge the gaps between scales? *Progress in Biophysics and Molecular Biology*, 107: 21–31, 2011.
- Carlos Ramos-Carreño. dcor: distance correlation and energy statistics in python, 3 2022. URL <https://github.com/vnmabus/dcor>.
- Alfréd Rényi. On measures of dependence. *Acta mathematica hungarica*, 10(3-4):441–451, 1959.
- Evangelos Sariyanidi, Casey J. Zampella, Evan DeJardin, John D. Herrington, Robert T. Schultz, and Bünyamin Tunç. Comparison of human experts and ai in predicting autism from facial behavior. In *CEUR Workshop Proceedings*, volume 3359, pp. 48–57, 2023.
- Evangelos Sariyanidi, Casey J. Zampella, Robert T. Schultz, and Bünyamin Tunç. Inequality-constrained 3d morphable face model fitting. *IEEE Transactions on Pattern Analysis and Machine Intelligence*, 46:1305–1318, 2024.
- Theodore D. Satterthwaite, John J. Connolly, Kosha Ruparel, Monica E. Calkins, Chad Jackson, Mark A. Elliott, David R. Roalf, Rachel Hopson, Karthik Prabhakaran, Melissa Behr, Hong Qiu, Frederick D. Mentch, Rosetta Chiavacci, Patrick M. A. Sleiman, Ruben C. Gur, Hakon Hakonarson, and Raquel E. Gur. The philadelphia neurodevelopmental cohort: A publicly available resource for the study of normal and abnormal brain development in youth. *NeuroImage*, 124:1115–1119, 2016.
- Alexander Schaefer, Ru Kong, Evan M. Gordon, Timothy O. Laumann, Xi-Nian Zuo, Avram J. Holmes, Simon B. Eickhoff, and B. T. Thomas Yeo. Local-global parcellation of the human cerebral cortex from intrinsic functional connectivity mri. *Cerebral Cortex*, 28:3095–3114, 2018.

-
- Richard C. Schmidt and Barbara O'Brien. Evaluating the dynamics of unintended interpersonal coordination. *Ecological Psychology*, 9:189–206, 1997.
- Richard C. Schmidt, Stephanie Morr, Paula Fitzpatrick, and Michael J. Richardson. Measuring the dynamics of interactional synchrony. *Journal of Nonverbal Behavior*, 36:263–279, 2012.
- Dino Sejdinovic, Bharath Sriperumbudur, Arthur Gretton, and Kenji Fukumizu. Equivalence of distance-based and rkhs-based statistics in hypothesis testing. *The Annals of Statistics*, 41:2263–2291, 2013.
- Lisa Shelley and Frank Gonzalez. Back channeling: Function of back channeling and l1 effects on back channeling in l2. *Linguistics Portfolio*, 2, 2013.
- Gábor J. Székely, Maria L. Rizzo, and Nail K. Bakirov. Measuring and testing dependence by correlation of distances. *The Annals of Statistics*, 35:2769–2794, 2007.
- Yonglong Tian, Dilip Krishnan, and Phillip Isola. Contrastive multiview coding. In *European conference on computer vision*, pp. 776–794. Springer, 2020.
- Paul H. Tiesinga and Terrence J. Sejnowski. Mechanisms for phase shifting in cortical networks and their role in communication through coherence. *Frontiers in Human Neuroscience*, 4:196, 2010.
- Dag Tjøstheim, Håkon Otneim, and Bjørn Støve. Statistical dependence: Beyond pearson's ρ . *Statistical Science*, 37, 2022.
- Sana Tonekaboni, Danny Eytan, and Anna Goldenberg. Unsupervised representation learning for time series with temporal neighborhood coding. *arXiv preprint arXiv:2106.00750*, 2021.
- Jakob Verbeek, Sam Roweis, and Nikos Vlassis. Non-linear cca and pca by alignment of local models. In *Advances in Neural Information Processing Systems 16*. MIT Press, 2003.
- Martin Vetterli, Jelena Kovačević, and Vivek K. Goyal. *Foundations of Signal Processing*. Cambridge University Press, 2014.
- Zhiguang Wang, Weizhong Yan, and Tim Oates. Time series classification from scratch with deep neural networks: A strong baseline. arXiv:1611.06455, 2016. URL <https://doi.org/10.48550/arXiv.1611.06455>.
- Marijke Welvaert and Yves Rosseel. On the definition of signal-to-noise ratio and contrast-to-noise ratio for fmri data. *PLoS ONE*, 8:e77089, 2013.
- Anderson M. Winkler, Gerard R. Ridgway, Gwenaél Douaud, Thomas E. Nichols, and Stephen M. Smith. Faster permutation inference in brain imaging. *NeuroImage*, 141:502–516, 2016.
- Gerald Woo, Chenghao Liu, Doyen Sahoo, Akshat Kumar, and Steven Hoi. Cost: Contrastive learning of disentangled seasonal-trend representations for time series forecasting. *arXiv preprint arXiv:2202.01575*, 2022.
- Kexin Zhang, Qingsong Wen, Chaoli Zhang, Rongyao Cai, Ming Jin, Yong Liu, James Y Zhang, Yuxuan Liang, Guansong Pang, Dongjin Song, et al. Self-supervised learning for time series analysis: Taxonomy, progress, and prospects. *IEEE transactions on pattern analysis and machine intelligence*, 46(10):6775–6794, 2024.
- Xinyu Zhang, Zhen Zhao, Theodoros Tsiligkaridis, and Marinka Zitnik. Self-supervised contrastive pre-training for time series via time-frequency consistency. In *Advances in Neural Information Processing Systems 35*, 2022.
- Ding-Xuan Zhou. Universality of deep convolutional neural networks. *Applied and Computational Harmonic Analysis*, 48:787–794, 2020.
- Xiaoqin Zhuang, Zening Yang, and Dietmar Cordes. A technical review of canonical correlation analysis for neuroscience applications. *Human Brain Mapping*, 41:3807–3833, 2020.

A NETWORK ARCHITECTURE, HYPERPARAMETERS AND IMPLEMENTATION

The transformations $f(\cdot)$ and $g(\cdot)$ are modelled with separate convolutional neural networks (CNNs), but both CNNs use an identical and well-established architecture. Specifically, each CNN is comprised of B identical blocks concatenated back to back. Each block is comprised of four layers:

- Batch normalization layer
- Convolutional layer
- Dropout
- ReLU

The convolutional layer has a stride parameter, which effectively downsamples the signals in time when it is greater than 1. Moreover, following standard practice, the convolutional layer at each block reduces the number of channels (i.e., dimension of signals) by half.

The training is done by using the Adam optimizer for 100 iterations (Table A.2), although the code has the option to stop early by using a certain percentage (default 20%) of the training data as a validation set. During training, we extract four randomly selected segment pairs from each signal pair. Each segment pair is picked to be concurrent (i.e., positive sample) with 50% probability and non-concurrent also with 50% probability.

We successfully used the network parameters in Table A.2 to expose dependencies on three types of biological signals with divergent characteristics –fMRI, physiological (ECG and respiration rate) and behavioral data– as well as the 100 synthesized datasets (Section 4.2). As such, these parameters have proven capability to expose a wide range of non-linear dependencies. If the two signals are dependent but through a large temporal lag, one may need to increase the number of blocks B . For example, we used the default parameter $B = 3$ successfully in a synthesized experiment where there was a lag of $\delta T = 500$ frames, but failed to capture dependence through a significantly larger amounts of lag (Fig. A.6). Nevertheless, setting the parameter to $B = 4$ allowed us to successfully capture such dependence through larger amounts of lags (e.g., a fixed lag of $\delta T = 1000$ or a variable lag between $\delta T \in [800, 1000]$). However, it must be noted that training a CNN also becomes more difficult as the number of blocks (i.e., depth) of the network increases. Thus, B cannot be increased arbitrarily, and therefore CNNs can not model very long range dependencies.

The number of output channels of the (first) convolution layer, C , controls the complexity of functions that can be modeled with f or g —the higher the C the more complex functions can be modeled. We set this parameter to $C = 512$, which worked successfully across a wide range of dependence patterns—from simple linear dependence between one-dimensional input segments to complex non-linear dependencies, including with multi-dimensional signals, such as in our experiments with behavioral data (82 dimensions). In other words, we did not observe any harm in setting this parameter to higher values than needed (e.g., linear dependence between one-dimensional signals could have been technically be exposed with $C = 1$ and $B = 1$). In cases where one deals with very high-dimensional input signals (e.g., in the order of hundreds or thousands) or one expects a very complex dependence,

Kernel size of first conv. layer	5
Kernel size of other conv. layers	3
Step size (stride) at conv. first layer	3*
Step size (stride) at other conv. layers	2*
Number of blocks (B)	3
Number of output channels at 1st conv. layer (C)	512
Number of output channels at b th conv. layer	$512/2^{(b-1)}$
Dropout rate	0.25
Optimizer	Adam ⁵¹
Number of iterations	100
Learning rate	10^{-4}

Table A.2: Parameters of the CNNs that we use. *The step sizes larger than 1 effectively downsample the input, and if the segment size w is too small, the output of a convolutional kernel may be empty. To avoid the latter, one may need to reduce the stride sizes accordingly.

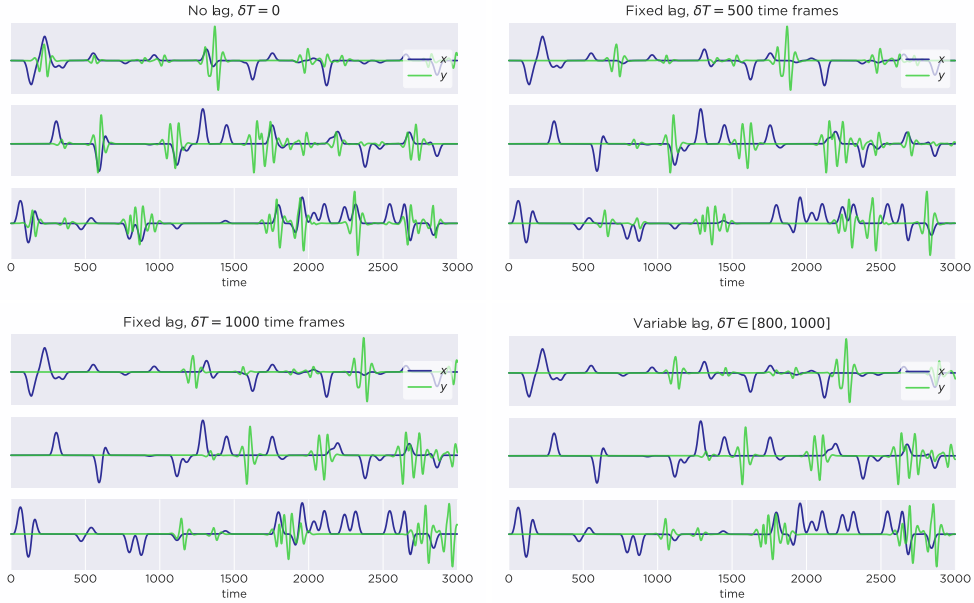


Figure A.6: Stochastically dependent signals with various amounts of lag. Top left: No lag ($\delta T = 0$). Top right: fixed lag of $\delta T = 500$ frames. Bottom left: fixed lag of $\delta T = 1000$. Bottom right: a random amount of lag between $\delta T \in [800, 1000]$.

one may need to set C to higher values than 512. Also, in cases where computational efficiency is a priority, one may reduce this value possibly without harm, since $C = 512$ is possibly a larger value than needed in many applications.

We implemented concurrence using `PyTorch`. With the default parameters, the concurrence coefficient on 500 pairs of signal pairs¹ of length $T = 1000$ can be computed in approximately 40s on a single NVIDIA GPU and requires approximately 500MB of memory. One can speed up the code by running fewer iterations (i.e., adjusting the `-num_iters` parameter) or reducing the number of channels C (i.e., the `-num_filters`).

Alongside the code, we also provide the 100 synthetic datasets that can be used to reproduce the synthetic experiment results for the Concurrence method.

B PROOF OF THEOREM 1

This section presents a series of remarks that lead to the proof of Theorem 1.

Remark 1. The processes $\tilde{\mathbf{h}}_x[t]$ and $\tilde{\mathbf{h}}_y[t]$ are Bernoulli processes.

Proof. The process $\tilde{\mathbf{h}}_x[t]$ defined as in equation 8 is equivalent to merging two processes (Bertsekas & Tsitsiklis, 2008), as it can also be written as

$$\tilde{\mathbf{h}}_x = \min\{\boldsymbol{\alpha}[t]\mathbf{h}[t] + \boldsymbol{\epsilon}_x[t], 1\} = \max\{\boldsymbol{\alpha}[t]\mathbf{h}[t], \boldsymbol{\epsilon}_x[t]\}. \quad (14)$$

Moreover, the processes that are being merged are both Bernoulli processes: The process $\boldsymbol{\alpha}[t]\mathbf{h}[t]$, which is Bernoulli as it is the product of two independent Bernoulli processes (Bertsekas & Tsitsiklis, 2008); and the error process $\boldsymbol{\epsilon}_x[t]$ which is Bernoulli by definition. Thus, $\tilde{\mathbf{h}}_x[t]$ is Bernoulli, as merging two Bernoulli processes leads to another Bernoulli processes (Bertsekas & Tsitsiklis, 2008). That the process $\tilde{\mathbf{h}}_y[t]$ is Bernoulli is can be proven with an analogous argument on the processes $\boldsymbol{\beta}[t]\mathbf{h}[t]$ and $\boldsymbol{\epsilon}_y[t]$. \square

¹Results are reported for the case where 80% of the data is used for training and the concurrence coefficient is computed on the remaining 20%.

Remark 2. Let \mathbf{c}^+ and \mathbf{c}^- be RSs that correspond to the sum terms of \mathbf{z}^+ and \mathbf{z}^-

$$\mathbf{c}^+[t] = \tilde{\mathbf{h}}_x[t]\tilde{\mathbf{h}}_y[t] \quad (15)$$

$$\mathbf{c}^-[t] = \tilde{\mathbf{h}}_x[t]\tilde{\mathbf{h}}_y[t + \tau']. \quad (16)$$

The RSs \mathbf{c}^+ and \mathbf{c}^- are Bernoulli processes with respective parameters

$$p^+ = pp_\alpha p_\beta + p_x^\epsilon p_y^\epsilon + pp_\alpha q_\beta q_x^\epsilon p_y^\epsilon + pq_\alpha p_\beta p_x^\epsilon q_y^\epsilon - pp_\alpha p_\beta p_x^\epsilon p_y^\epsilon \quad (17)$$

$$p^- = p^2 p_\alpha p_\beta + p_x^\epsilon p_y^\epsilon + pp_\alpha q_\beta q_x^\epsilon p_y^\epsilon + pq_\alpha p_\beta p_x^\epsilon q_y^\epsilon - p^2 p_\alpha p_\beta p_x^\epsilon p_y^\epsilon + pq p_\alpha p_\beta (p_y^\epsilon q_x^\epsilon + p_x^\epsilon q_y^\epsilon), \quad (18)$$

where q , q_α , q_β , q_x^ϵ and q_y^ϵ are defined as $q = 1 - p$, $q_\alpha = 1 - p_\alpha$, $q_\beta = 1 - p_\beta$, $q_x^\epsilon = 1 - p_x^\epsilon$, $q_y^\epsilon = 1 - p_y^\epsilon$

Proof. The process $\mathbf{c}^+[t]$ is the product two Bernoulli processes, and it is Bernoulli itself as it takes binary values (0 or 1) and its outcome at different times are independent,

$$P\{\mathbf{c}^+[t_1], \mathbf{c}^+[t_2]\} = P\{\mathbf{c}^+[t_1]\}P\{\mathbf{c}^+[t_2]\}, \quad (19)$$

since all the processes involved in the computation of $\mathbf{c}^+[t]$ (i.e., $\alpha[t]$, $\beta[t]$, $\mathbf{h}[t]$, $\epsilon_x[t]$, $\epsilon_y[t]$) are independent from t . The parameter of p^+ of the Bernoulli process $\mathbf{c}^+[t]$ can be computed by noting that $\mathbf{c}^+[t]$ takes the value 1 in the presence of four events: (i) When $\alpha[t]$, $\beta[t]$ and $\mathbf{h}[t]$ all take the value 1; or (ii) when the error processes $\epsilon_x[t]$ and $\epsilon_y[t]$ both take the value 1; or (iii) when $\mathbf{h}[t]$, $\alpha[t]$, $\epsilon_y[t]$ take the value 1 but $\beta[t]$ and $\epsilon_x[t]$ take the value 0; or (iv) when $\mathbf{h}[t]$, $\beta[t]$, $\epsilon_x[t]$ take the value 1 but $\alpha[t]$ and $\epsilon_y[t]$ take the value 0. Thus, the parameter p^+ of the Bernoulli process \mathbf{c}^+ is calculated as in equation 17—the first four terms in equation 17 account for the four aforelisted events, and the last (negative) term ensures that the event of all five processes ($\mathbf{h}[t]$, $\alpha[t]$, $\beta[t]$, $\epsilon_x[t]$ and $\epsilon_y[t]$) taking the value 1 is not accounted for twice. With a similar argument, it can be shown that \mathbf{c}^- is a Bernoulli process with the parameter p^- calculated as in equation 18. \square

Remark 3. If the parameter p of the process $\mathbf{h}[t]$ is in the range $(0, 1)$ as in equation 11, then

$$p^+ > p^-. \quad (20)$$

Proof. By rewriting the first term of p^+ in equation 18 as $pp_\alpha p_\beta = p^2 p_\alpha p_\beta + pq p_\alpha p_\beta$, the difference between p^+ and p^- can be shown to be

$$p^+ - p^- = p_\alpha p_\beta pq(1 - p_y^\epsilon q_x^\epsilon - p_x^\epsilon q_y^\epsilon) - pp_\alpha p_\beta p_x^\epsilon p_y^\epsilon (1 - p) \quad (21)$$

$$= p_\alpha p_\beta pq(1 - p_y^\epsilon q_x^\epsilon - p_x^\epsilon q_y^\epsilon) - pp_\alpha p_\beta p_x^\epsilon p_y^\epsilon q \quad (22)$$

$$= p_\alpha p_\beta pq(1 - p_x^\epsilon q_y^\epsilon - p_y^\epsilon q_x^\epsilon - p_x^\epsilon p_y^\epsilon) \quad (23)$$

The term $p_\alpha p_\beta pq$ is strictly positive due to the assumptions in equation 11. The term $(1 - p_x^\epsilon q_y^\epsilon - p_y^\epsilon q_x^\epsilon - p_x^\epsilon p_y^\epsilon)$ is also strictly positive, as

$$1 = (p_x^\epsilon + q_x^\epsilon)(p_y^\epsilon + q_y^\epsilon) = p_x^\epsilon p_y^\epsilon + p_x^\epsilon q_y^\epsilon + q_x^\epsilon p_y^\epsilon + q_x^\epsilon q_y^\epsilon \quad (24)$$

$$\implies 1 - p_x^\epsilon q_y^\epsilon - p_y^\epsilon q_x^\epsilon - p_x^\epsilon p_y^\epsilon = q_x^\epsilon q_y^\epsilon, \quad (25)$$

and the assumptions in equation 11 guarantee that $q_x^\epsilon q_y^\epsilon$ is also strictly positive. Since $p^+ - p^-$ is the product of two positive terms, we have that $p^+ - p^- > 0 \implies p^+ > p^-$. \square

Remark 4. The \mathbf{z}^+ and \mathbf{z}^- defined in equation 12 are scaled Binomial random variables with mean and variance

$$\mathbb{E}\{\mathbf{z}^+\} = p^+ \quad (26)$$

$$\mathbb{E}\{\mathbf{z}^-\} = p^- \quad (27)$$

$$\text{Var}(\mathbf{z}^+) = \frac{1}{w} p^+ q^+ \quad (28)$$

$$\text{Var}(\mathbf{z}^-) = \frac{1}{w} p^- q^-, \quad (29)$$

where $q^+ = 1 - p^+$ and $q^- = 1 - p^-$.

Proof. The RV $\tilde{\mathbf{z}}^+$ defined as $\tilde{\mathbf{z}}^+ = w\mathbf{z}^+$ is Binomial with mean and variance $\mathbb{E}\{\tilde{\mathbf{z}}^+\} = wp^+$ and $\text{Var}(\tilde{\mathbf{z}}^+) = wp^+q^+$, as $\tilde{\mathbf{z}}^+$ is the sum of w independent Bernoulli variables (Remark 2) with parameter p^+ . Since \mathbf{z}^+ is a version of $\tilde{\mathbf{z}}^+$ that is scaled by $\frac{1}{w}$, the mean $\mathbb{E}\{\mathbf{z}^+\}$ is obtained by multiplying $\mathbb{E}\{\tilde{\mathbf{z}}^+\}$ by $\frac{1}{w}$ and the variance $\text{Var}(\mathbf{z}^+)$ is obtained by multiplying $\text{Var}(\tilde{\mathbf{z}}^+)$ by $\frac{1}{w^2}$, verifying equation 26 and equation 28. One can use an analogous argument to verify that \mathbf{z}^- is scaled a Binomial RV with mean and variance as in equation 27 and equation 29. \square

Proof of Theorem 1. Equations equation 20, equation 26 and equation 27 together prove the first claim made in Theorem 1, namely, that the mean of \mathbf{z}^+ is greater than that of \mathbf{z}^- for any positive integer w . Equation 13 are proven by using equation 23 and equation 25. Furthermore, according to equation 28 and equation 29, the variance of both \mathbf{z}^+ and \mathbf{z}^- approaches zero as $w \rightarrow \infty$, which means that the distributions of \mathbf{z}^+ and \mathbf{z}^- become increasingly narrow as w increases. The latter implies that the distributions of \mathbf{z}^+ and \mathbf{z}^- become increasingly more disjoint as w increases, suggesting that the second claim made in Theorem 1 also holds—that there exists a threshold value θ such that $P\{\mathbf{z}^+ < \theta\} \rightarrow 0$ and $P\{\mathbf{z}^- > \theta\} \rightarrow 0$ as $w \rightarrow \infty$. A formal proof can be given by using the Chebyshev inequality as below.

Suppose that δ is defined as the fixed parameter

$$\delta = \frac{p^+ - p^-}{2}. \quad (30)$$

Then, according to Chebyshev inequality, the probability $P\{|\mathbf{z}^+ - \mathbb{E}\{\mathbf{z}^+\}| > \delta\} = P\{|\mathbf{z}^+ - p^+| > \delta\}$ is bounded above by

$$P\{|\mathbf{z}^+ - p^+| > \delta\} \leq \frac{1}{\delta^2} \text{Var}(\mathbf{z}^+) = \frac{1}{\delta^2 w} p^+ q^+. \quad (31)$$

Since w appears in the denominator of the upper bound in equation 31 and all p^+, p^- are positive constants, it holds that this bound

$$\frac{1}{\delta^2 w} p^+ q^+ \rightarrow 0 \text{ as } w \rightarrow \infty. \quad (32)$$

Since $\frac{1}{\delta^2 w} p^+ q^+$ is an upper bound for the probability $P\{|\mathbf{z}^+ - p^+| > \delta\}$, it also holds that $P\{|\mathbf{z}^+ - p^+| > \delta\} \rightarrow 0$ as $w \rightarrow \infty$. The probability $P\{|\mathbf{z}^+ - p^+| > \delta\}$ can be written as $P\{|\mathbf{z}^+ - p^+| > \delta\} = P\{\mathbf{z}^+ - p^+ > \delta\} + P\{p^+ - \mathbf{z}^+ > \delta\}$. Since both terms $P\{\mathbf{z}^+ - p^+ > \delta\}$ and $P\{p^+ - \mathbf{z}^+ > \delta\}$ are probabilities, they are nonnegative by definition, therefore their sum $P\{|\mathbf{z}^+ - p^+| > \delta\}$ can approach zero only if both of them approach zero:

$$P\{\mathbf{z}^+ - p^+ > \delta\} \rightarrow 0 \text{ as } w \rightarrow \infty \quad (33)$$

$$P\{p^+ - \mathbf{z}^+ > \delta\} \rightarrow 0 \text{ as } w \rightarrow \infty. \quad (34)$$

By constructing an analogous argument for the RV \mathbf{z}^- , one can show that

$$P\{\mathbf{z}^- - p^- > \delta\} \rightarrow 0 \text{ as } w \rightarrow \infty \quad (35)$$

$$P\{p^- - \mathbf{z}^- > \delta\} \rightarrow 0 \text{ as } w \rightarrow \infty. \quad (36)$$

Equations equation 34 and equation 35 can be rearranged as

$$P\{p^+ - \delta > \mathbf{z}^+\} \rightarrow 0 \text{ as } w \rightarrow \infty \quad (37)$$

$$P\{\mathbf{z}^- > \delta + p^-\} \rightarrow 0 \text{ as } w \rightarrow \infty. \quad (38)$$

By using the definition of δ in equation 30, one can establish that

$$p^+ - \delta = \delta + p^- = \frac{p^+ + p^-}{2}. \quad (39)$$

Thus, the value $\theta = \frac{p^+ + p^-}{2}$ can replace the thresholds $p^+ - \delta$ and $p^+ + \delta$ in equation 37 and equation 38, completing the proof of Theorem 1:

$$P\{\theta > \mathbf{z}^+\} \rightarrow 0 \text{ and } P\{\mathbf{z}^- > \theta\} \rightarrow 0 \text{ as } w \rightarrow \infty.$$

\square

C NUMERICAL SIMULATIONS

We present numerical simulations that illustrate the main theoretical result of our study, namely, that concurrent and non-concurrent segments extracted from signal pairs must be separable if the signals are statistically dependent. The separability is expected to increase as the gap between the distributions \mathbf{z}^+ and \mathbf{z}^- increases. According to equation 23 and equation 25, the difference between the means of \mathbf{z}^+ and \mathbf{z}^- is

$$p^+ - p^- = p_\alpha p_\beta p q q_x^\epsilon q_y^\epsilon, \quad (40)$$

which suggests that the separability between concurrent and non-concurrent segments is expected to increase when:

- The dependence between $\mathbf{x}[t]$ and $\mathbf{y}[t]$ gets stronger (i.e., p_α and p_β increase)
- The estimation error in $\tilde{\mathbf{h}}_x[t]$ or $\tilde{\mathbf{h}}_y[t]$ decreases (i.e., q_x^ϵ or q_y^ϵ increase).

We present numerical simulations through computer-generated signals from the processes $\mathbf{h}[t]$, $\tilde{\mathbf{h}}_x[t]$ and $\tilde{\mathbf{h}}_y[t]$ introduced in the previous section. We also investigate whether the concurrent and non-concurrent segments are expected to be separable when the stationarity assumption for the process $\mathbf{h}[t]$ is violated, by including simulations with a time-varying parameter $p(t)$ for the process $\mathbf{h}[t]$. Specifically, we present results from the five scenarios listed in Table C.1. Examples of the generated signals are listed in Fig. C.1.

Fig. C.2 illustrates the results of the experiments where we computed empirical distributions of the RVs \mathbf{z}^+ and \mathbf{z}^- computed according to five different scenarios, namely, the **(a)**–**(b)** of Table C.1. The results in Fig. C.2 indicate that the main outcome of Theorem 1 holds even when the simplifying assumption of Bernoulli processes is abandoned, as \mathbf{z}^+ and \mathbf{z}^- are separable even when they are derived from non-stationary variables and their overlap reduces as the segment size w increases.

D SIGNIFICANCE TEST WITH PEARSON TYPE III APPROXIMATION

To avoid spurious discoveries (i.e., Type-I error) with the application of the proposed framework, we advise users to conduct permutation tests for assessing statistical significance. The null distribution that we use for significance testing is the distribution of concurrence coefficients compared by randomly permuting the positive and negative labels (i.e., concurrent and non-concurrent segments) used during the computation of the concurrence coefficient. While the concurrence coefficient is defined by clipping the classification accuracy so that 50% represents minimal accuracy,

$$\text{concurrence coefficient} = 2 \times \max\{0.5, \text{classification accuracy}\} - 1, \quad (41)$$

for the purposes of significance testing, we use the unclipped concurrence coefficient (UCC) defined simply as

$$\text{UCC} = 2 \times \text{classification accuracy} - 1, \quad (42)$$

to preserve the integrity of the null distribution's shape. The classification accuracy of randomly assigned positive and negative segments is expected to lead to a Gaussian-like distribution centered

Table C.1: The five dependence scenarios used for the numerical simulations in Fig. C.2.

- (a)** Deterministic dependence ($p_\alpha=p_\beta=1$) with perfect recovery ($p_x^\epsilon = p_y^\epsilon = 0$).
 - (b)** Stochastic dependence ($p_\alpha=p_\beta=0.5$) with perfect recovery.
 - (c)** Stochastic dependence ($p_\alpha=p_\beta=0.5$) with imperfect recovery ($p_x^\epsilon=p_y^\epsilon=0.5$)
 - (d)** Deterministic dependence with perfect recovery, but through a non-stationary process $\mathbf{h}[t]$, where the probability of $\mathbf{h}[t] = 1$ increases linearly with t .
 - (e)** Stochastic dependence ($p_\alpha = p_\beta = 0.5$) with imperfect recovery ($p_x^\epsilon = p_y^\epsilon = 0.5$) and through a non-stationary process $\mathbf{h}[t]$ as in case **(d)**.
-

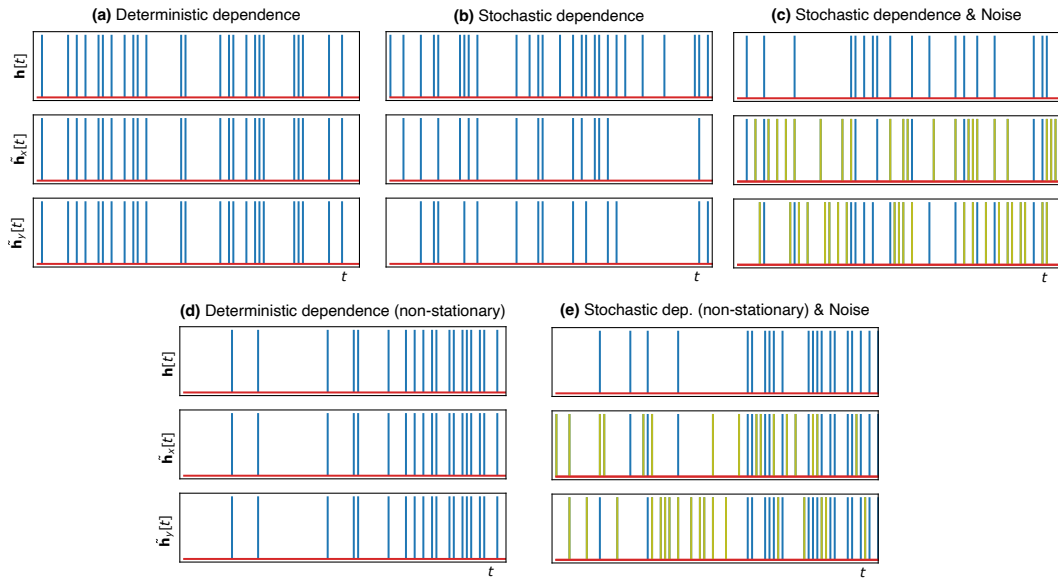


Figure C.1: Illustrations of (dependent) binary signals. We illustrate the estimated processes $\tilde{h}_x[t]$ and $\tilde{h}_y[t]$ together with the common underlying process $h[t]$ for five different cases, representing the five scenarios (a)-(e) listed in Table C.1.

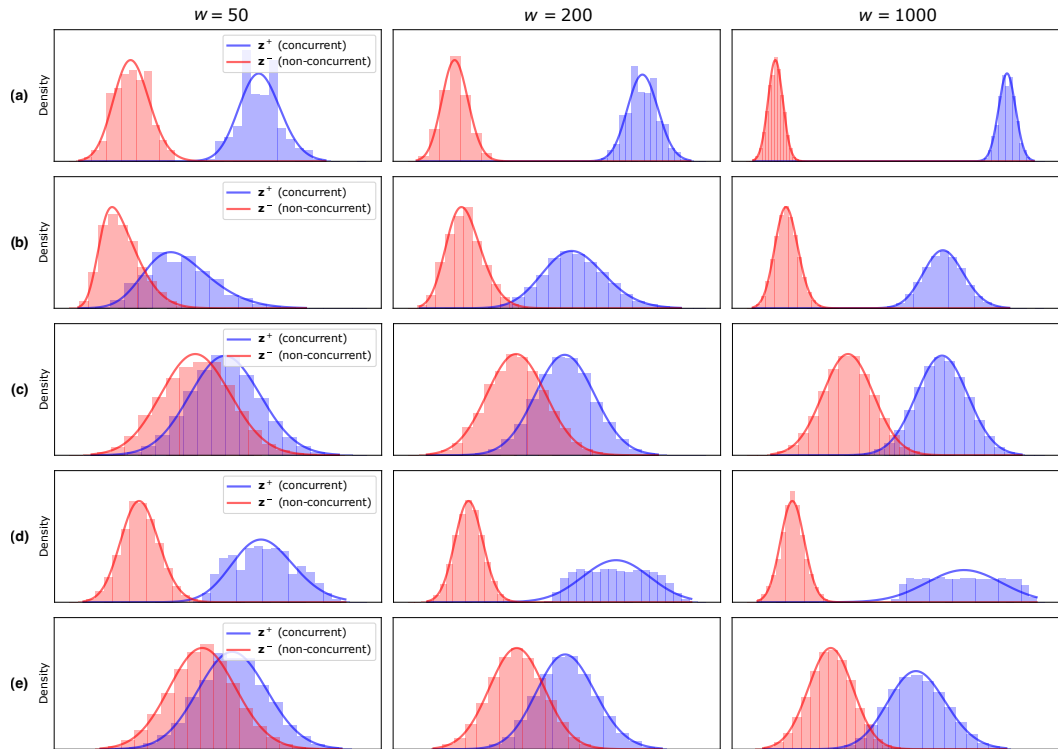


Figure C.2: Numerical simulations showing that concurrent and non-concurrent segments are separable across a variety of dependence scenarios. The labels (a-e) correspond to the scenarios depicted in Table C.1 and Fig. C.1.

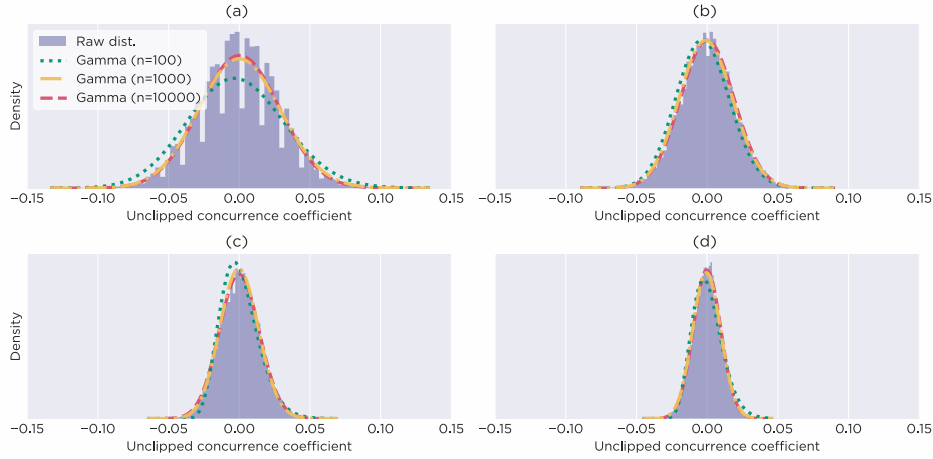


Figure D.1: The null distribution used for significance testing. Permutation tests for when the (unclipped) concurrence coefficient (UCC) is computed from 20, 50, 100 or 200 signal pairs, after randomly assigning the positive/negative labels to the segment pairs that are used for computing the concurrence coefficient. We show the histograms of raw UCC values, and also the Pearson Type III (i.e., shifted and scaled Gamma) distributions that are fit to n raw values ($n = 100, 1000, 10000$). As expected⁵², the null distribution generally gets more narrow as the UCC is computed from an increasing number of samples.

50%⁵², and the UCC allows us to observe whether this is the case for the classifier that underlies the concurrence coefficient.

Fig. D.1 shows the distribution (i.e., histogram) of 10000 UCC values computed by extracting concurrent and non-concurrent pairs of segments from a dataset of dependent signal pairs, randomly assigning a label (positive or negative) to each segment pair, and then fitting a Pearson Type III distribution to these values using ML. Specifically, we plot three separate Pearson Type III distributions obtained by fitting to 100, 1000 and 10000 UCC values. Results show that the UCC follows a Gauss-like distribution, and that, as expected⁵², the variance of this distribution reduces as the UCC is computed from larger samples. The Pearson Type III distribution computed from 1000 values very closely approximates the distribution computed from 10000 permutations in all four plots in Fig. D.1.

E ILLUSTRATION OF RANDOM SEQUENCES USED IN THEORETICAL ANALYSES

Fig. E.1 shows realizations of the random sequences (RSs) that underlie for our theoretical analysis (equations 4-7). The first row illustrates the binary (Bernoulli) process $\mathbf{h}[t]$ that renders the RSs \mathbf{x} and \mathbf{y} dependent. The second and third row illustrate the binary processes $\mathbf{h}_x[t]$ and $\mathbf{h}_y[t]$, which are the events that \mathbf{x} and \mathbf{y} respond to. The fourth and fifth row show the results of convolution of the binary RSs $\mathbf{h}_x[t]$ and $\mathbf{h}_y[t]$ with two separate kernels k_1 and k_2 . The next two rows show independent noise processes, and the final two rows indicate the resulting RSs \mathbf{x} and \mathbf{y} .

F ILLUSTRATION OF RESULTS ON BEHAVIORAL APPLICATION

Fig. F.1 illustrates the application of concurrence to behavioral signals, which involves comparison of multi-dimensional signals (Fig. F.1a,b). The per-segment-concurrence-score (PSCS) computed from the sample of adolescents shows that behavioral coordination increases with age, and that its degree differs between people with autism and neurotypical development.

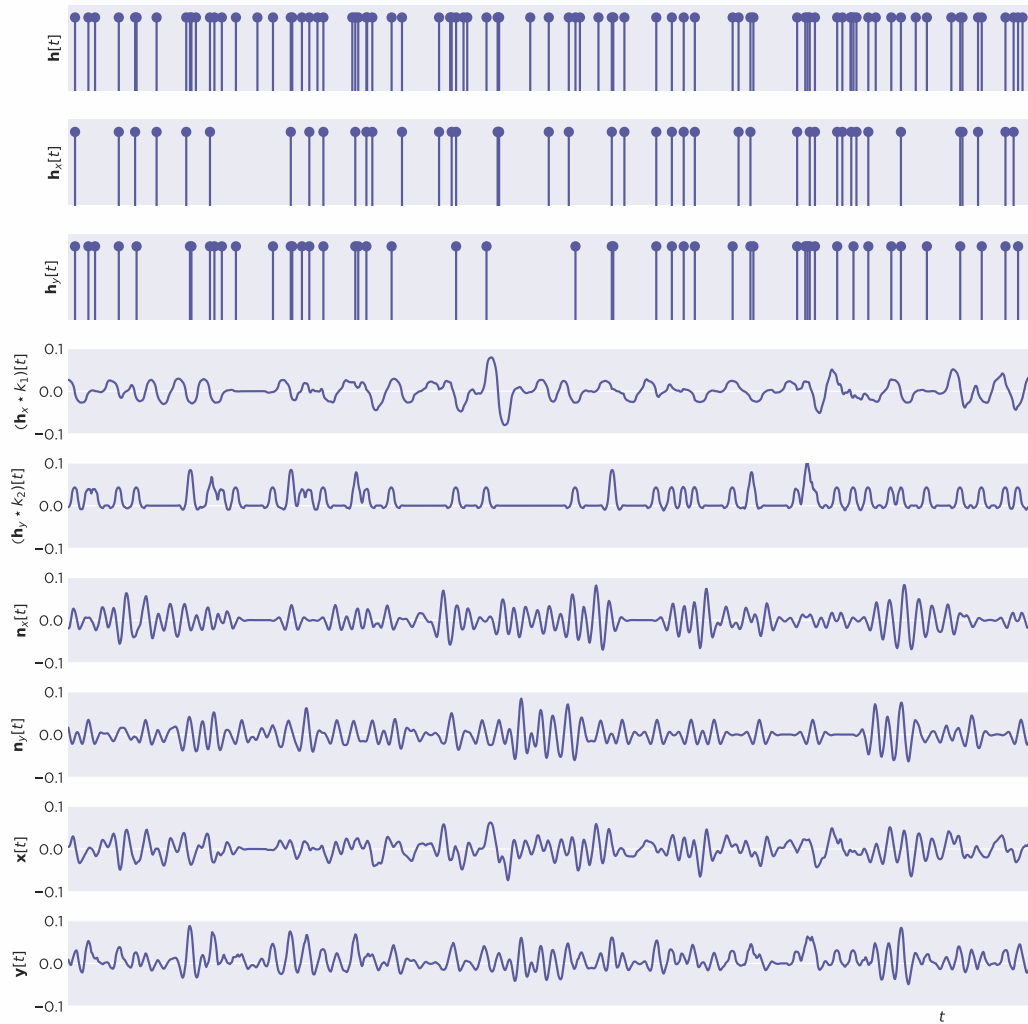


Figure E.1: Signal pairs generated according equations 4-7. The last two rows show an example pair of signals (i.e., realizations of $x[t]$ and $y[t]$ in equation 4 and equation 5), and the rows above them show the underlying impulse processes $h[t]$, $h_x[t]$, $h_y[t]$, and the noise processes $n_x[t]$ and $n_y[t]$.

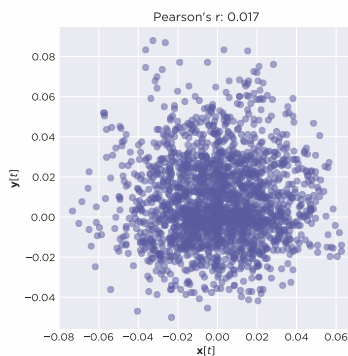


Figure E.2: Scatter plot of the realizations of x and y illustrated in Fig. E.1. The signals are dependent albeit approximately uncorrelated (Pearson's $r = 0.017$).

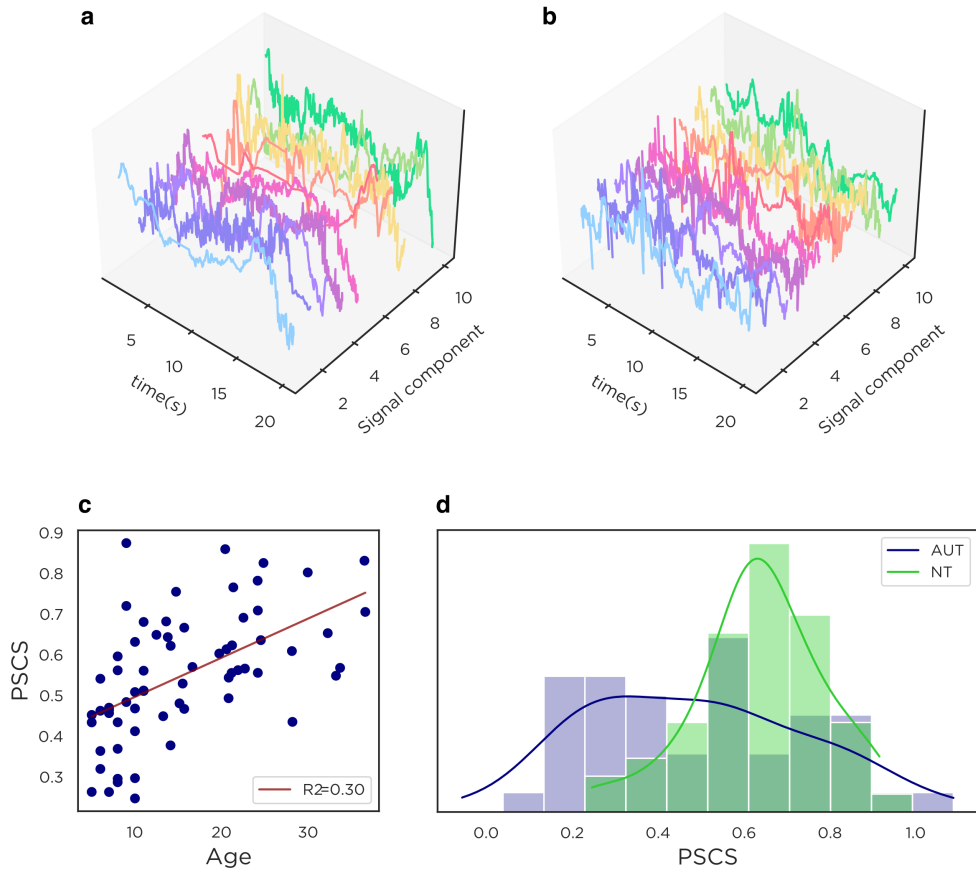


Figure F.1: (a) Multi-dimensional signals from the participant during a conversation. (b) Multi-dimensional signals from the confederate during the same conversation. (c) Average per-segment concurrence score (PSCS) per neurotypical (NT) individual versus age. (d) The distributions of PSCS per individual for the autism (AUT) and NT group.